Journal of Power Sources 560 (2023) 232594

Contents lists available at ScienceDirect

Journal of Power Sources

journal homepage: www.elsevier.com/locate/jpowsour

Using nickel-molybdenum cathode catalysts for efficient hydrogen gas production in microbial electrolysis cells

Ruggero Rossi *, Joseph Nicolas, Bruce E. Logan

Department of Civil and Environmental Engineering, The Pennsylvania State University, University Park, PA, 16802, USA

HIGHLIGHTS

- NiMo catalyst for hydrogen evolution reaction was synthesized by different routes.
- Hydrothermal route (NiMoHt) had superior performance than electrochemical synthesis.
- Using NiMo Ht in an MEC enabled large current densities and H_2 production rates.
- A novel configuration enabled inclusion of a reference electrode.
- Cathode resistance dominated (70%) over MEC internal resistance.

ARTICLE INFO

Keywords:
Microbial electrolysis cell
Biohydrogen
NiMo catalyst
Anode and cathode resistance
AEM

ABSTRACT

A low-cost cathode catalyst based on a NiMo alloy was examined here to replace noble metals for the hydrogen production in microbial electrolysis cells (MECs). Two NiMo catalysts were synthesized through either an electrochemical assisted (NiMo Elec) or a hydrothermal (NiMo Ht) approach. The NiMo Ht method enriched the electrocatalyst with Mo atoms compared to the NiMo Elec approach, producing a similar current density with a minimal overpotential of 50 mV compared to Pt. In MEC tests using the NiMo Ht catalyst, H_2 was generated at a highest rate of 81 ± 3 L_{H2}/L-d (current density of 44.4 ± 0.9 A/m^2) at a cell voltage of −0.86 V, and a Coulombic efficiency of >97%. Modifying the closely stacked MEC design to include a reference electrode, and analysis of the electrode potentials using the electrode potential slope method, revealed a large contribution of the cathode resistance (5.3 ± 0.5 mΩ m^2) compared to the anode (1.4 ± 0.2 mΩ m^2) and ohmic resistance (0.83 mΩ m^2) for a total internal resistance of 7.6 ± 0.5 mΩ m^2. The high performance of the NiMo Ht catalyst coupled with its low cost provides an economically viable approach to advance the generation of biohydrogen in MECs.

1. Introduction

Microbial electrolysis cells (MECs) leverage the microbial metabolism at the anode to generate electrons for evolving hydrogen at the cathode [1–3]. The exoelectrogenic microbes on the anode oxidize the organic matter in solution and release to a conductive electrode the electrons, which are then delivered to the cathode, where they are used to produce hydrogen gas by the hydrogen evolution reaction (HER) [4,5]. While carbon-based electrodes are typically preferred as anode materials due to their high biocompatibility and tunable chemical and physical properties such as surface area [6,7], there is no consensus on the optimal cathode catalyst for MECs [8]. Pt-based catalysts are typically used due to their high activity toward H_2 generation in water electrolyzer [9,10]. However, their high cost, susceptibility to contamination, and fouling in the complex media used in MECs, has limited their scalability and widespread adoption [11,12]. Ni, stainless steel, Mo, Cu and Mg are inexpensive alternatives that have been examined in several MEC studies, with Ni-based catalysts being the most popular among these [8]. Ni represents the state-of-the-art catalyst for water electrolysis under alkaline conditions, due to its high chemical stability ad low cost [13]. However, in MECs Ni-based catalysts have had much lower performance than those using precious metal catalysts, resulting in overpotentials larger than 100 mV at high current densities [14,15]. While Mo alone does not represent an efficient catalyst for the HER due to the high energy of the Mo–H bond, Ni–Mo alloys could potentially reduce cathode overpotentials in MECs as this material couples the

* Corresponding author.
E-mail address: rxr57@psu.edu (R. Rossi).

https://doi.org/10.1016/j.jpowsour.2022.232594
Received 18 August 2022; Received in revised form 5 December 2022; Accepted 26 December 2022
Available online 27 January 2023

stability of Ni atoms with the high Mo activity towards HER [16–20].

To fully exploit the potential of improved cathode catalysts MEC configurations are needed that limit the development of mass-transfer limitations and minimize ohmic resistance while enabling high performance of the cell. Reactor configuration can have a large impact on MEC performance, primarily affecting the ohmic resistance and the development of mass-transfer limitations in the cell [21–23]. Cubic reactors or systems with large spacing between the electrodes have the advantage of allowing easy inspection and monitoring through reference electrode of the MEC operation but are a poor choice for achieving optimal electrochemical reactor performance (i.e. reducing energy requirements). A large spacing between the electrodes increases the ohmic resistance of the cell due to the large distance the ions travel in solution to balance the charge transported by the electrons [24]. A large electrode spacing, combined with a solution conductivity, produces an ohmic resistance that can account for more than one third of the overall internal resistance of some reactors [23,25]. Large electrode spacings can also produce mass-transfer limitations in the cell that result in pH imbalances. At the anode, protons released during oxidation of the organic matter accumulate due to sodium and potassium primarily balancing charges in solution (Na^+ and $K^+ \sim 50$ mM; $H^+ = 0.1$ μM) in solution. At the cathode, hydroxide ions are produced by the HER but the preferential transport of other negative ions such as Cl^- or $H_2PO_4^-$ due to their larger concentration (Cl^- and $H_2PO_4^- \sim 50$ mM; $H^+ = 0.1$ μM), facilitate their accumulation on the electrode surface. As a result of the preferential transport of ions in solution in sub-optimal designs, the pH at the anode decreases while the pH at the cathode increases [26]. A low local anode pH limits the activity of the bioanode, as the tolerance of microorganisms for low pH is limited, reducing the maximum current density of the MEC [27], while a high local cathode pH increases the voltage requirement, according to the Nernst equation, reducing the energy efficiency of the system [28,29].

A zero-gap MEC configuration, with an anion exchange membrane (AEM) separator and a gas cathode chamber, can be used to avoid pH changes and reduce internal resistances. This new MEC design has enabled the best MEC performance to date, producing up to 43.1 ± 0.6 A/m^2 and 72 ± 2 L_{H2}/L-d in 50 mM phosphate buffer at a cell voltage of 0.79 V, using a Pt/C cathode catalyst [30]. The zero-gap spacing between the electrodes, separated only by the membrane, minimized the ohmic resistance while the absence of a liquid catholyte enabled the selective transport of hydroxide ions from cathode to anode, boosting the current density by reducing pH acidification at the anode and diminishing cell voltage requirements. However, that MEC used a precious metal catalyst (Pt), and it was not possible to insert a reference electrode into the system to measure the individual contributions of the anode, cathode, and solution/membrane resistance to the total internal resistance [13]. Recent research on AEM water electrolyzers has shown that NiMo catalysts are the most active catalysts for the HER under highly alkaline conditions, leveraging Ni atoms as excellent water dissociation centers, coupled with Mo atoms providing superior adsorption properties towards hydrogen [16–20]. In this study, we examined the use of novel Ni-Mo based cathode alloys as catalysts [31] in a zero-gap MEC reactor configuration where near-neutral local anode pH can be maintained [30], boosting the electrochemical performance. NiMo catalysts were prepared using two different techniques, and the impact of the NiMo synthesis method on the cathode performance under both abiotic conditions (electrochemical tests) and in MECs was examined. The NiMo catalyst was prepared using a fast and straightforward electron-assisted approach [32,33] and compared with a hydrothermal synthesis that was recently implemented to produce the best precious metal free HER catalyst in an AEM water electrolyzer [31]. Hydrothermal syntheses have been previously used to produce catalysts with defined structures, composition, and superior catalytic performance [34,35]; however, the high number of steps of the synthesis and the use of sensitive equipment increases time and cost over simpler electrodeposition preparations. Typical zero-gap configuration, due to the lack of space, do not allow to insert a reference electrode in the system to monitor anode and cathode performance. Here, by modifying the reactor configuration to include an additional port for the reference electrode on the anode end plate, it was possible for the first time to monitor the anode and cathode performance over time during a polarization test, enabling the identification of the limiting electrochemical steps by the electrode potential slope (EPS) analysis [21,23].

2. Materials and methods

2.1. Catalyst preparation

The NiMo catalysts was prepared using two different approaches: electrode assisted synthesis (NiMo Elec), and a hydrothermal process (NiMo Ht) (Fig. 1). For the electrochemical approach, 0.17 M $NiCl_2$ hexahydrate, 0.10 M Na_2MoO_4 dihydrate and 0.17 M sodium citrate were mixed in a beaker and the pH was adjusted to 10 using NH_4OH following a previously published method [36]. A mixed metal oxide (1 cm^2) was used as the anode and placed 1 cm apart from a graphite block (1 cm^2) cathode. Under vigorous stirring, a current of 1 A was applied over 4–5 h to favor the precipitation of a NiMo alloy on the graphite cathode (Fig. S1). The metal deposit was gently scraped from the surface, collected, dried in a vacuum oven at 70 C for 30 min and micronized in a ball mill using 5 mm diameter zirconia balls for approximately 24 h.

Hydrothermal synthesis was performed by mixing 0.05 M $NiCl_2$ hexahydrate with 0.05 M Na_2MoO_4 dihydrate in a 150 mL stainless steel autoclave in deionized water. The autoclave was heated in a muffle furnace set at 160 C for 6 h and cooled to room temperature inside the furnace. The green precipitate ($NiMoO_4$) produced was then filtered and washed with deionized water, collected, dried in a vacuum oven at 70 C for 30 min and micronized in a ball mill using 5 mm diameter zirconia balls for approximately 24 h. The NiMo precursor was then heat-treated in a tubular furnace at 550 C under a 95% N_2 – 5% H_2 reducing atmosphere for 2 h as previously described [31] (Fig. S2).

2.2. Catalyst characterization

NiMo catalysts were examined using X-ray photoelectron spectroscopy (XPS) (Physical Electronics VersaProbe III) with a monochromatic Al kα x-ray source ($h\nu = 1486.6$ eV) and a concentric hemispherical analyzer. Charge neutralization was performed using both low energy electrons (<5 eV) and argon ions. The binding energy axis was calibrated using sputter cleaned Cu (Cu 2p3/2 = 932.62 eV, Cu 3p3/2 = 75.1 eV) and Au foils (Au 4f7/2 = 83.96 eV) [37]. Peaks were charge referenced to CH_x band in the carbon 1s spectra at 284.8 eV. Measurements were made at a takeoff angle of 45° with respect to the sample surface plane resulting in a typical sampling depth of 3–6 nm (95% of the signal originated from this depth). Quantification was done using instrumental relative sensitivity factors that account for the x-ray cross section and inelastic mean free path of the electrons.

After catalyst immobilization on the carbon cloth cathode, the electrode was analyzed using scanning electron microcopy (SEM) (Verios G4, Thermo-Scientific, Hillsboro, OR) with an accelerating voltage of 5 keV and a current of 0.1 nA. EDS spectra were collected using a X-MaxN detector (Oxford Instruments, Concord, MA) at an accelerating voltage of 5 keV and a current of 3.2 nA. Aztec (Version 5.0) software was used to analyze the EDS data.

2.3. Cathode and membrane electrode assembly preparation

The cathodes and membrane electrode assemblies (MEAs) were prepared by spraying Pt/C or NiMo catalysts on a carbon cloth support (Fuel Cell Store, 5% wet proofed). The catalysts contained Pt dispersed in carbon (20% Pt, 80% C; Fuel Cell Store) or NiMo dispersed in carbon black (Vulcan XC-72-R, Fuel Cell Store). The impact of catalyst loading

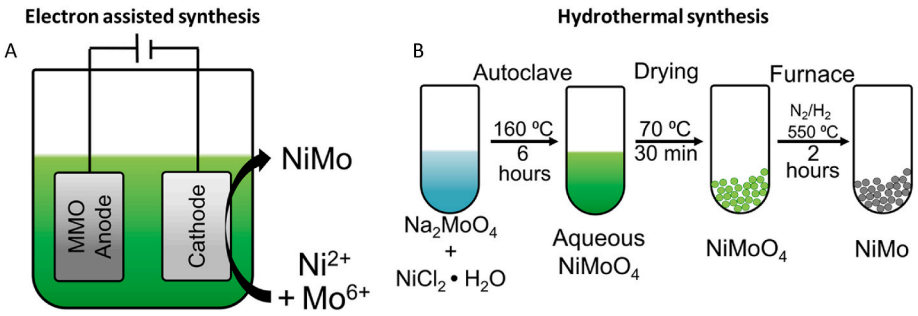

Fig. 1. Schematic of the NiMo catalyst synthesis using (A) an electron assisted method and (B) a hydrothermal synthesis.

was examined using NiMo loadings of 2 mg_{NiMo}/cm^2, 3 mg_{NiMo}/cm^2, 4 mg_{NiMo}/cm^2, and 5 mg_{NiMo}/cm^2 by varying the NiMo/C ratio in the catalyst ink. The thickness of the catalyst layer was maintained consistent by always spraying the same amount of catalyst on the electrode support and changing the catalyst/carbon ratio (Fig. S3). To prepare the catalyst ink, 100 mg of catalyst dispersion (Pt/C or NiMo/C) were mixed with 500 mg of deionized water and 1700 mg of isopropanol under vigorous stirring. The ionomer (Fumion FAA-3-SOLUT-10, Fuel Cell Store) was added dropwise to the solution. The impact of ionomer content on cathode performance was investigated by using four different ionomer concentration of 0.5 mg/cm^2, 1 mg/cm^2, 2.5 mg/cm^2 and 5.0 mg/cm^2 (Fig. S4), and then used 2.5 mg/cm^2 in subsequent tests. These concentrations correspond to 5%, 10%, 25% and 50% of the concentration of dispersion (catalyst + carbon) in the ink. The ink was sonicated for 1 h at room temperature before being sprayed on a carbon cloth taped to a hot plate set to 80 C to a final loading of approximately 2 mg/cm^2 of metal using an air brush and compressed N_2 gas (0.8 atm). The cathodes were then dried overnight under a fume hood and tested as is in the abiotic electrochemical tests or cold pressed at 35 °C onto the AEM (two thicknesses of 75 μm, Fumasep FAA-3-PK-75; and 50 μm, Fumasep FAA-3-50; Fuel Cell Store) at 306 atm for 3 min to develop the final membrane electrode assembly (MEA) to be used in the MEC.

2.4. Electrochemical tests

All abiotic electrochemical tests were conducted in a cubic cell 4 cm long with a diameter of 3 cm and an empty volume of 28 mL with the cathode as the working electrode and a Pt mesh (3 cm^2 projected area) as a counter electrode, placed 3 cm far from the cathode. The reference electrode (RE) used to measure the electrode potentials (Silver chloride (Ag/AgCl) reference electrode; BASI; +199 mV versus a standard hydrogen electrode, SHE) was placed in the current path between the working and the counter electrode, 1 cm distant from the cathode. All the individual electrode potentials are reported here versus SHE and have been corrected for the ohmic resistance except otherwise noted. An anion exchange membrane (Selemion AMVN, Asahi Glass, Co., Tokyo, Japan) was used to separate the working and the counter electrode (Pt) to minimize contamination of the catholyte.

Cathodic linear sweep voltammetries (LSVs) were conducted from the open circuit potential (OCP) to −3 V at a scan rate of 1 mV s^{-1}. Prior to LSVs the working electrodes were left for 2 h at the OCP and then a fast electrochemical impedance spectroscopy (EIS) analysis (from 100 kHz to 500 Hz, 10 mV amplitude, 10 points s^{-1}) was recorded at the OCP to calculate the solution resistance (R_Ω) [22]. Reported electrode potentials were corrected by adjusting the measured potential based on the ohmic resistance obtained from EIS [24]. Carbon felt anodes (3 mm thick, Alfa Aesar) were acclimated in cubic reactors as previously described at an applied potential of 0.2 V for more than one month before being transferred in the flow through MEC with closely spacing electrodes [30]. The current density was calculated by normalizing the current by the geometric cross-sectional area of the cell (A = 7 cm^2). The performance of the anodes was compared to previously published work using the EPS method by linearizing a portion of the cell potential over a range of current density and measuring the electrical resistance in units of mΩ m^2 [21–23]. The y-intercepts on the potential axis was used to calculate the experimental open circuit potentials.

2.5. MEC assembly and operation

The MEC was assembled as previously described [30], except it was modified to include a reference electrode (Fig. S6). Briefly, the acclimated carbon felt anode was sandwiched with the MEA in a zero-gap cell. Two rubber gaskets (3 mm thickness) were used in the anode and cathode chambers, the anode chamber was completely occupied by the carbon felt while the cathode chamber was filled with a set of three plastic spacers placed between teh cathode and the end plate to maintain a zero-gap spacing between the electrodes. The total reactor volume was 4.5 mL based on the empty anode and cathode chambers. Sodium acetate (2 g/L) in phosphate buffer 50 mM (PBS, 4.58 g L^{-1} Na_2HPO_4, 2.45 g L^{-1} $NaH_2PO_4{\cdot}H_2O$, 0.31 g L^{-1} NH_4Cl, 0.13 g L^{-1} KCl; σ = 7 mS/cm) amended with vitamin and mineral solutions was continuously recirculated in the anode chamber at a flow rate of 10 mL/min (theoretical hydraulic retention time, HRT = 14 s) and replaced daily unless otherwise specified. The anolyte was sparged with N_2 for approximately 15 min before using it. There was no catholyte in the MEC and the headspace of a sealed glass container filled with deionized water was recirculated at 5 mL/min (HRT = 27 s) in the cathode chamber to avoid gas accumulation past the cathode and provide water through the vapor stream for the HER. Deionized water used to develop a vapor feed at the cathode (never replaced) was sparged with N_2 for approximately 15 min to remove oxygen from the solution only prior to startup of the MEC on day 1. To investigate the electrode performance in polarization tests, a novel MEC design was developed that allowed insertion of a reference electrode in the anode chamber. A threaded insert was added in the anode end plate and a low-profile Ag/AgCl reference electrode (RRPEAGCL – Pine Research) was used to monitor the electrode potential over time. A photo of the cell is reported in the Supporting Information.

The MEC voltage was controlled through a power supply (3646A, Circuit Specialists) and the current was continuously monitored from the voltage drop measured across a 10 Ω resistor (R_{ext}) connected in series with the MEC. The voltage of the MEC (V_{cell}) and the voltage applied by the instrument before R_{ext} (V_{app}) were continuously recorded every 20 min using a Keithley 2700. V_{app} includes the voltage loss across the external resistor used to calculate the current produced by the MEC, while V_{cell} represents the actual cell voltage. The applied voltage was changed from −0.8 V to −1.2 V at 0.1 V steps (V_{cell} from −0.67 V to −0.86 V). Each applied voltage was maintained for at least 48 h. The whole cell and the individual electrode performance were analyzed using the EPS method as previously described [21]. The MEC ohmic resistance (R_Ω), including solution, membrane and wiring R_Ω in the assembled MEC was calculated using EIS. Current was normalized by the reactor cross-sectional area (7 cm^2).

The volume and purity of gas produced at the cathode was analyzed

using a gas chromatograph (SRI Instrument) equipped with a molecular sieve column. The gas volume produced was calculated following a previous method and compared with the theoretical H_2 production rate based on the coulombs generated during each cycle to calculate the cathode Coulombic efficiency [38]. The hydrogen production rate was calculated by normalizing the volume of H_2 produced for the overall MEC empty volume of 4.5 mL (anode + cathode chambers). The anode Coulombic efficiency was calculated as previously described based on the coulombs produced and the chemical oxygen demand (COD, TNTplus COD reagent; HACH) consumed [39].

3. Results and discussion

3.1. NiMo material properties

XPS analysis of the two samples indicated that the Mo:Ni ratio on the Ht sample was approximately 5× larger compared to the Elec sample, indicating an enrichment in Mo through the hydrothermal approach (Fig. 2, Table 1). In the Ht sample, approximately three Mo atoms were present on the surface for each Ni atom, while in the Elec sample, for each Mo atom two Ni atoms were present on the metal. In NiMo alloys for HER, the catalytic activity is primarily due to the Mo atoms on the surface, which leverage their d-band electronic structure similar to Pt to enable hydrogen evolution at high rate [9]. According to a previous study, the Ni and the NiMo facilitate the activity of the Mo atoms on the surface, providing a conductive support and optimal adsorption properties for hydrogen [40]. Additionally, in the Elec sample, the portion of oxidized Ni was larger compared to the Ht sample, indicating a thicker oxide structure and thus likely a less conductive catalyst. Previous studies have reported that diminishing the oxide layer thickness on a Ni-based electrocatalysts, decreased the overpotential and boosted the electrochemical activity, likely by increasing the conductivity of the alloy [41].

The NiMo catalyst immobilized on a carbon cloth analyzed by SEM (Fig. 3) showed that the NiMo in the NiMo Ht sample was evenly distributed over the surface of the catalyst (Fig. 3C) compared to the formation of large NiMo clusters in the NiMo Elec sample (Fig. 3D). The difference in the catalyst distribution over the carbon cloth support was likely due to the different percentages of Ni and Mo in the catalysts and the possible interactions between the catalyst particles during ink preparation and spraying. If the metal clusters are not effectively dispersed during ink preparation, they can produce visible aggregations (Fig. 3D). During the Elec cathode preparation, the NiMo particles were assembling together, the main reason for the strong interaction between the NiMo Elec particles is not known. The NiMo Ht sample did not produce visible particle aggregates, and thus the catalyst appeared to be more evenly spread over the electrode (Fig. 3C). The SEM-EDS analysis revealed, in accordance with XPS, a larger ratio of Mo:Ni in the Ht sample compared to Elec (Fig. S7). However, the ratio was slightly smaller for the SEM-EDS analysis compared to XPS, likely due to the different sampling depth of the two techniques. This smaller ratio suggests a slightly variable elemental composition in function of the thickness and the fact that the XPS samples were pure NiMo while the EDS analysis was conducted on the blended NiMo/C catalyst sprayed on the carbon cloth and immobilized with the ionomer.

3.2. Electrochemical characterization of the cathode catalysts

Analysis of the LSVs revealed a large impact of the catalyst composition on the cathode electrochemical performance (Fig. 4A). The

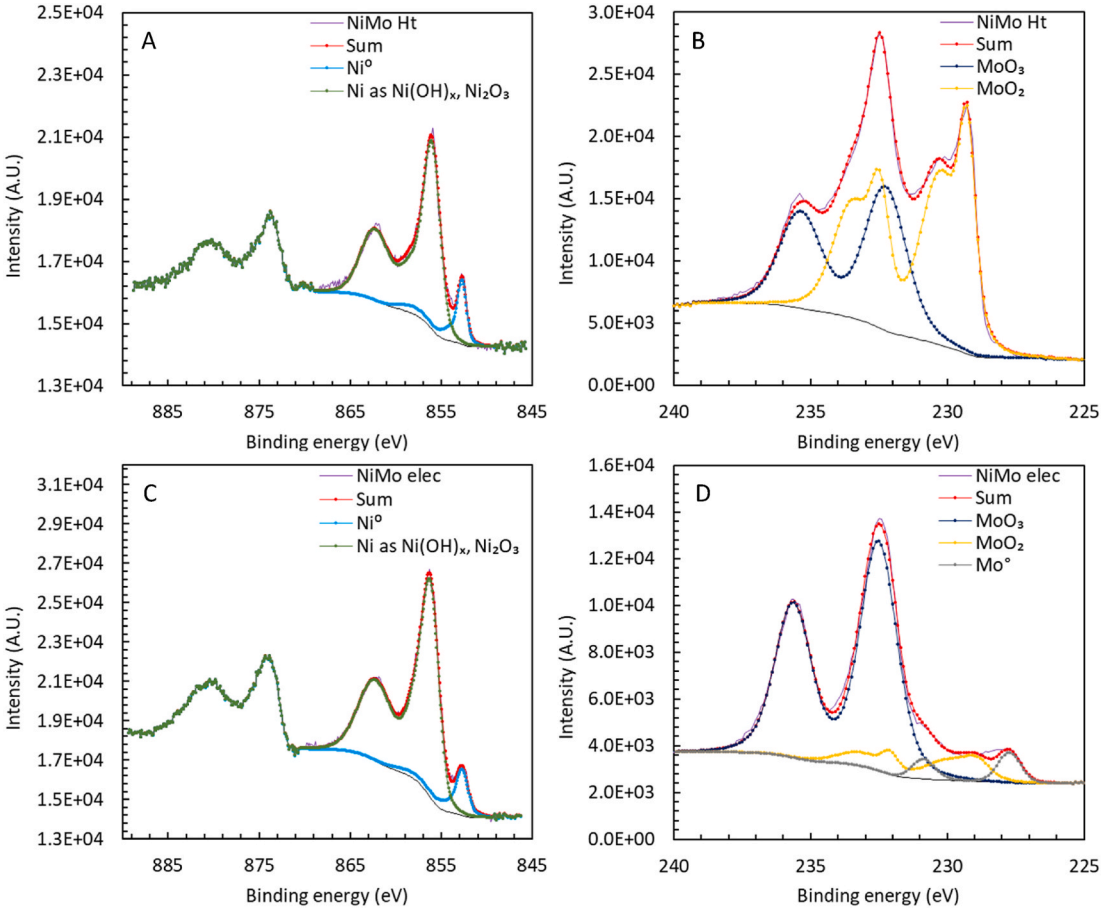

Fig. 2. XPS spectra of the NiMo catalyst prepared using (A, B) a hydrothermal synthesis (NiMo Ht) and (B, D) an electron assisted method (NiMo Elec).

Table 1
Concentration of element in the prepared samples in atomic percentage.

	Molybdenum				Nickel				
Sample	Mo^{total}	Mo°	MoO_2	MoO_3	Ni^{total}	Ni as Ni(OH) $_x$, Ni_2O_3	Ni metal	O	Mo:Ni
NiMo Ht	24.4	/	15.1	9.3	8.0	6.9	1.1	58.8	3.1
NiMo Elec	10.7	0.6	1.2	8.1	17.0	15.1	1.9	58.3	0.6

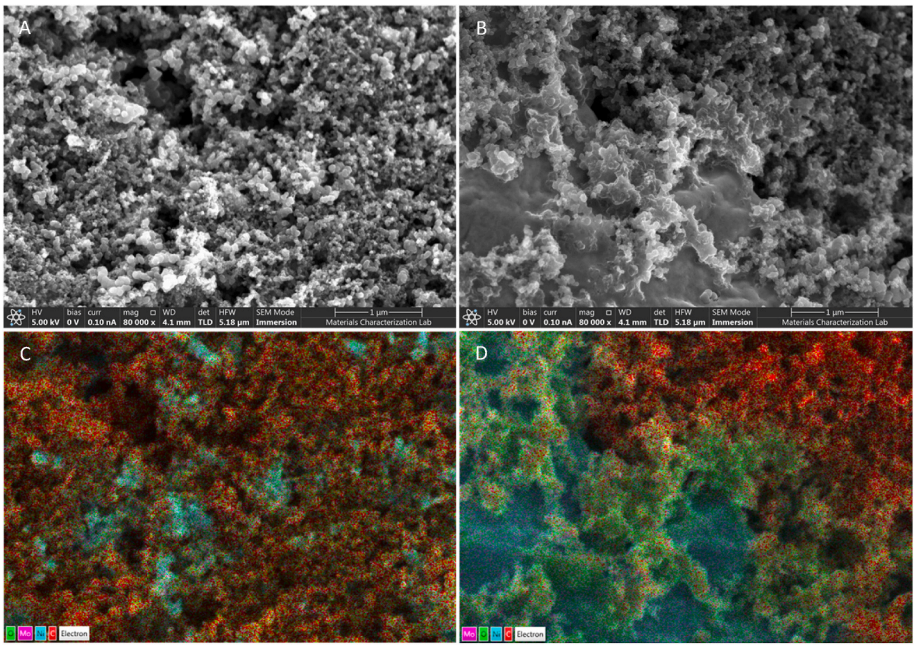

Fig. 3. (A, B) SEM and (C, D) EDS mapping for O, Mo, Ni and C distribution of the NiMo catalyst sprayed on the carbon cloth prepared using (A, C) a hydrothermal preparation and (B, D) an electron assisted method. In the EDS photos C is colored in red, O in green, Ni in turquoise and Mo in purple. (For interpretation of the references to color in this figure legend, the reader is referred to the Web version of this article.)

performance of the different catalysts was investigated using a similar loading (except for the pure carbon black, CB sample, where no catalyst was added) of 2 mg/cm^2. NiMo Ht and Pt/C represented the best catalysts, producing the lowest overpotentials between the series, followed by NiMo Elec and CB. At 40 A/m^2, the electrode potential for NiMo Ht was −0.87 ± 0.00 V, approximately 120 mV more negative than that of Pt/C (−0.75 ± 0.00 V). NiMo Elec required an electrode potential of −1.02 ± 0.02 V at 40 A/m^2, 17% percent larger than NiMo Ht while in the absence of catalyst the electrode potential was −1.22 ± 0.01 V, 40% larger than NiMo Ht, indicating the superior activity of NiMo Ht for the HER compared to the other non-precious metal catalysts (Fig. 4B). The high activity of the NiMo Ht catalyst compared to NiMo Elec were likely due to the larger Mo content of the catalyst, as shown by the XPS and EDS analysis. Previous studies indicated that Mo plays a major role in HER catalysis likely due to the similar d-band electronic structure with Pt and represent the most active catalyst when blended with Ni [9]. The metallic Ni and the NiMo complexes provide a conductive matrix to the oxidized Mo species on the surface, preventing dissolution and modifying the electronic structure of the Mo, which catalyze the HER [40].

Increasing the catalyst loading from 2 mg/cm^2 to 3 mg/cm^2 reduced the electrode overpotential by 70 mV at a current density of 40 A/m^2, from −0.87 ± 0.00 V (2 mg/cm^2) to −0.80 ± 0.01 V (Fig. 4C). Further increasing the NiMo loading did not produce any significant increase of the catalytic activity. The NiMo Ht potential at 40 A/m^2 with a catalyst loading of 3 mg/cm^2 was only 50 mV more negative than the Pt/C at the same current density with a loading of 2 mg/cm^2, indicating that a lower electrochemical activity of the NiMo Ht compared to Pt can be compensated in part by larger catalyst loading on the cathode.

3.3. MEC performance using precious metal free cathodes

The MEC using NiMo Ht as a cathode catalyst produced an average current density of 44.4 ± 0.9 A/m^2 over a one-day cycle at a cell voltage of V_{cell} = –0.86 V (V_{app} = 1.2 V) (Fig. 5A). Reducing the cell voltage diminished the driving force for the electrochemical reactions and thus decreased the current density. For example, the current density decreased to 37.2 ± 0.5 A/m^2 at −0.82 V, and to 30.1 ± 0.8 A/m^2 at −0.78 V. The maximum current density was stable over a one-day cycle and for consecutive cycles at different applied voltages. After 19 days from startup, at the maximum current density, the cycle length was extended to investigate the impact of the organic matter content on the MEC performance. The maximum current density remained stable over three consecutive days (from day 19 to day 22) at 45.0 ± 0.4 A/m^2 and then quickly decreased to 32 ± 3 A/m^2 after substrate was substantially depleted from the recycled anolyte, as indicated by a chemical oxygen demand in the solution below 229 ± 15 mg/L. Previous studies indicated that a minimum COD concentration larger than ~200 mg/L is needed in bioelectrochemical systems to sustain current generation and avoid large decrease in performance [42].

The average current density at each applied voltage was used to generate the polarization curve of the MEC (Fig. 5B). The MEC internal resistance was 6.9 ± 0.4 mΩ m^2 and the minimum cell voltage to generate H_2 was −0.56 ± 0.01 V (onset voltage). In a previous study using the same MEC configuration with Pt/C as a cathode catalyst, the internal resistance was 6.8 ± 0.3 mΩ m^2 with an onset voltage of −0.50 V [30], indicating the impact of the cathode catalyst. This comparison shows that replacing Pt with NiMo increased the onset voltage by approximately 60 mV, which is in reasonable agreement with our LSV

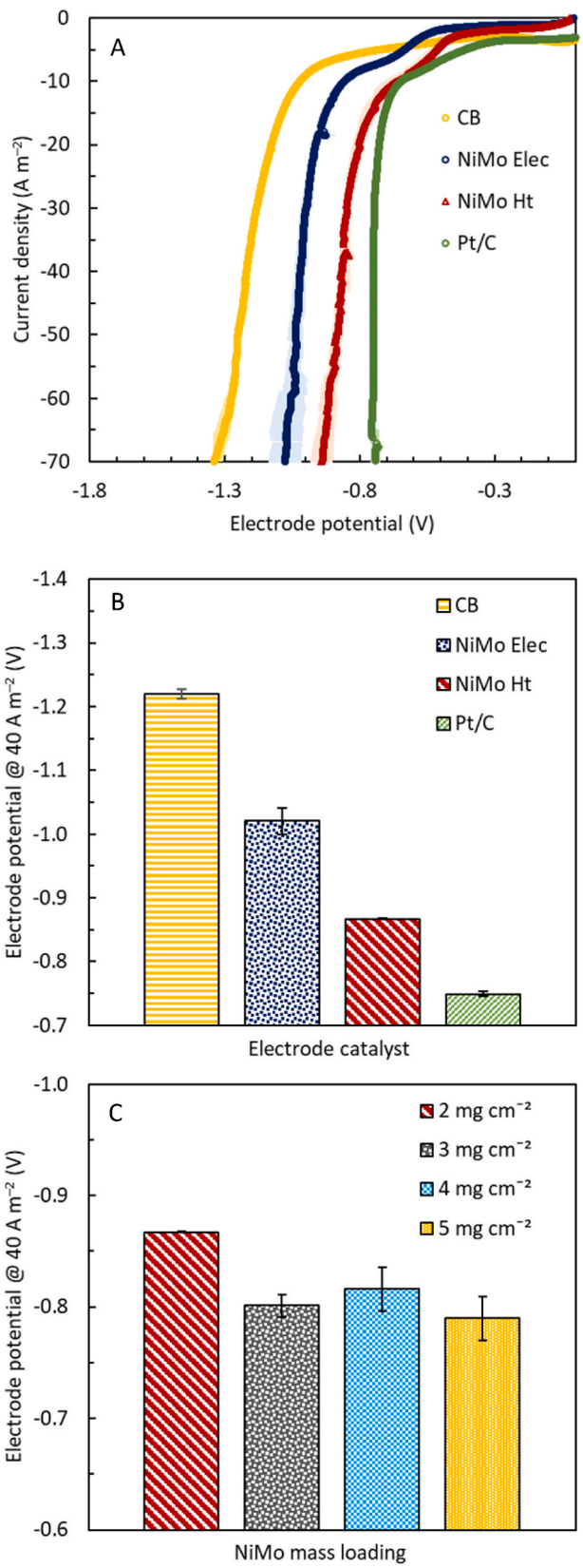

Fig. 4. (A) Electrochemical performance of the NiMo catalyst prepared using an electron assisted method (NiMo Elec) and a hydrothermal preparation (NiMo Ht) compared to carbon black (CB) and Pt/C LSVs. (B) Electrode potential at 40 A m^{-2} after IR correction. (C) Impact of NiMo Ht loading on the electrode performance.

data showing that the NiMo Ht cathodes required 50 mV additional voltage to sustain a current density of 40 A/m^2 compared to Pt/C.

The MEC had an excellent rate of high purity H_2 gas production with a Coulombic efficiency that approached 100% (Fig. 5C). At the lowest cell voltage of −0.86 V, the volumetric H_2 production rate was 81 ± 3 L_{H2}/L-d. This production rate was 13% larger than that previously obtained using a Pt/C cathode (72 ± 2 L_{H2}/L-d) [30], likely due to the slightly larger current density of the MEC using NiMo (44.4 ± 0.9 A/m^2, E_{cell} = −0.86 V) compared to the previous MEC using a Pt catalyst (43.2 ± 1 A/m^2, E_{cell} = −0.79 V). More positive cell voltages reduced the current densities and diminished the H_2 production rate. For example, H_2 productivity was 48 ± 4 L_{H2}/L-d at a cell voltage of −0.78 V and further decreased to 29 ± 1 L_{H2}/L-d at −0.67 V. The high H_2 production rate was due to the large current density of the cell and an average cathodic Coulombic efficiency of 97 ± 4% for all the cell voltage investigated. The anodic Coulombic efficiency was 98 ± 5% on average at all cell voltages, likely due to the absence of oxygen in the cell and the small anode chamber volume completely occupied by the anode carbon felt, which likely limited the growth of competitive cultures and enable a selective oxidation of acetate to electrons in the anode.

3.4. Using a reference electrode in the zero-gap MEC to monitor the electrode performance

To investigate the specific impact of the NiMo Ht catalyst on the MEC performance, the cell design was successfully modified to accommodate a reference electrode in close contact with the anode carbon felt (Fig. S6). A custom-made reference electrode was inserted through the anode end-plate to monitor the anode and cathode potential as the cell voltage was gradually changed over time (from V_{cell} = −0.69 V to V_{cell} = −0.94 V) (Fig. 5D, Fig. S8). At the most negative voltage the maximum current density was 48.2 ± 0.2 A/m^2 which was higher than that previously obtained in the absence of a reference electrode, even though a more positive voltage range was applied (from −0.67 V to −0.86 V). More negative voltages were not applied to avoid damaging the bioanode, as previously shown [30]. The inclusion of the reference electrode slightly increases the MEC internal resistance from 6.9 ± 0.4 mΩ m^2 to 7.6 ± 0.5 mΩ m^2, with no appreciable impact on the onset voltage (−0.57 ± 0.02 V). Based on the EPS analysis, the cathode resistance was 5.3 ± 0.5 mΩ m^2, representing 70% of the MEC resistance while the anode resistance was 1.4 ± 0.2 mΩ m^2, corresponding to only 18% of the total internal resistance. The remaining 0.83 mΩ m^2 (11%) was due to ohmic and membrane resistance.

These results indicate that cathode resistance, which is typically dominated by the kinetics of the HER, is primarily controlling the MEC performance in the current density range examined here. Previous studies have shown that the cathode resistance quickly decreases as more negative voltages are applied and more current is produced. However, the bioanode overpotential does not just continuously increase with applied voltages as it cannot sustain large current densities and the bioanode fails if the cell voltage is set too negative [22]. Thus, future studies would need to consider both methods to avoid anode failure at high current densities while at the same time improving the cathode kinetics at low current densities in order to reduce the internal resistance.

3.5. Impact of membrane thickness on MEC performance

Reducing the membrane thickness from 75 μm to 50 μm produced a minimal decrease in the MEC total internal resistance from 6.9 ± 0.4 mΩ m^2 to 6.0 ± 0.6 mΩ m^2 (Fig. 6A and B). The decrease in the internal resistance was due to the lower ohmic resistance of the cell, as shown by the EIS analysis (Fig. 6C). For example, the ohmic resistance measured with EIS decreased by an average of 47 ± 14% over the whole cell voltages, although the membrane thickness was decreased by 33% from 75 μm to 50 μm. A slightly higher onset voltage was obtained in the MEC

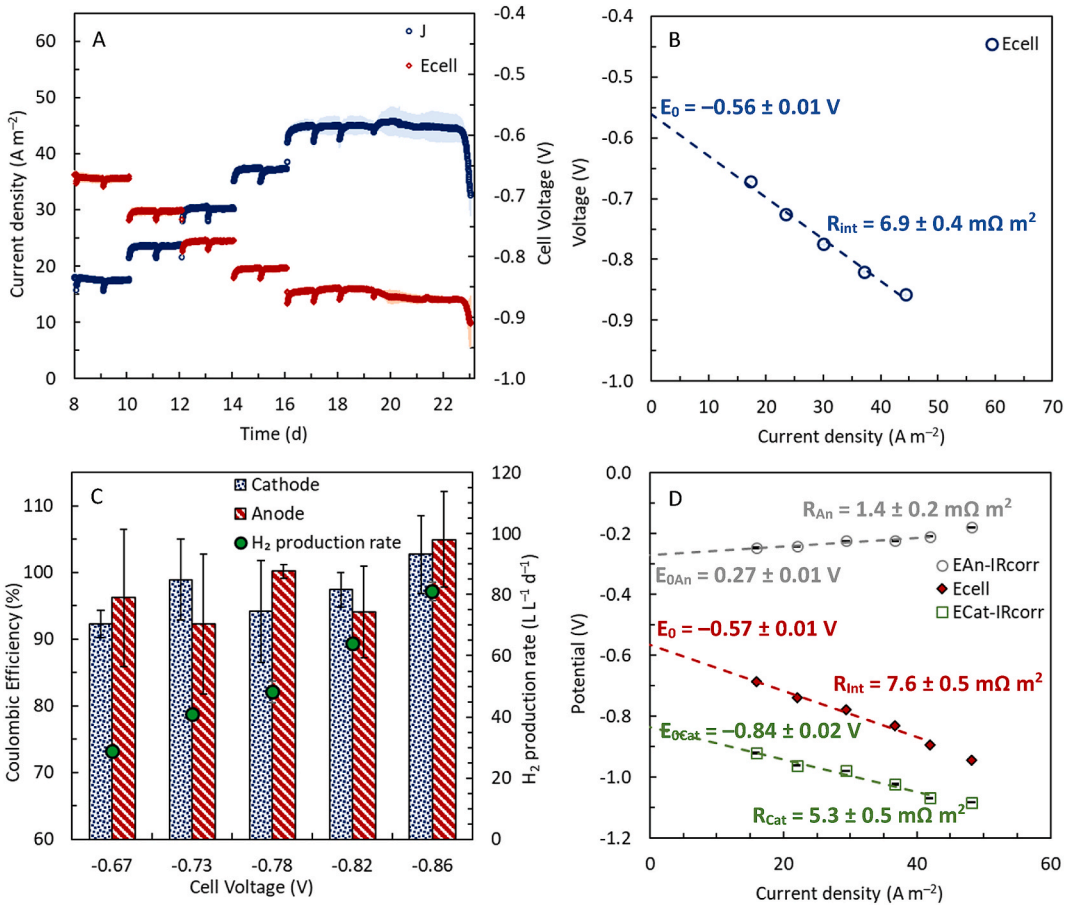

Fig. 5. MEC performance using NiMo Ht as a cathode catalyst. (A) MEC voltage (E_{cell}) and produced current density (J) over time using NiMo catalyst and (B) corresponding polarization curve. (C) Anodic and cathodic coulombic efficiency and hydrogen production rate. (D) Anode (An), cathode (Cat), and cell potential monitored with a reference electrode. Anode and cathode potentials were corrected for the ohmic resistance.

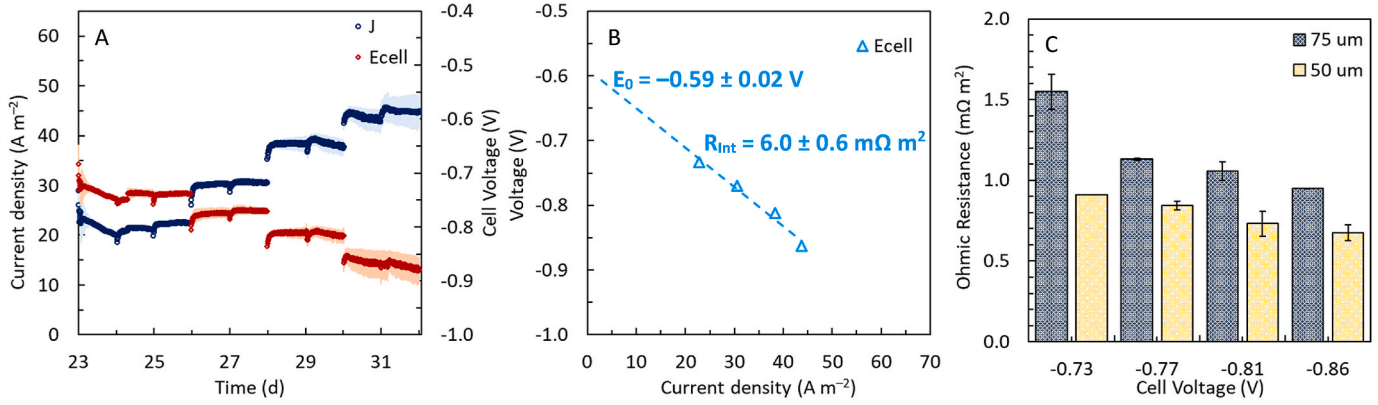

Fig. 6. Impact of membrane thickness on the MEC performance. (A) MEC voltage and produced current density over time using a thin (50 μm) AEM and (B) corresponding polarization curve. (C) Comparison of the MEC ohmic resistance using a 50 μm and 75 μm AEM.

with a 50 μm membrane (−0.59 ± 0.02 V), however, it was not significantly different from the onset voltage obtained with the 75 μm membrane (−0.56 ± 0.01 V) based on the overlap of the standard deviations.

3.6. Cost-performance analysis

The performance of precious metal free MEC presented in this study was among the highest performance achieved in MEC with similar configuration and solution chemistry, and was higher than other MECs using more concentrated buffer and substrate. The maximum current density of the NiMo Ht MEC was 48.2 ± 0.2 A/m^2 in the polarization curve, which is 12% higher than 43.2 ± 1.1 A/m^2 previously obtained using a Pt/C cathode even though a more positive cell voltage of −0.79 V was applied in that study compared to −0.94 V here [30]. The high current density coupled with Coulombic efficiencies >97% translated in a H_2 production rate of 81 ± 3 L_{H2}/L-d, which was 13% larger than that previously obtained using a Pt/C cathode (72 ± 2 L_{H2}/L-d).

Reducing the catalyst cost in MEC is fundamental and an important path forward for scaling up this technology. The largest portion of the cost in synthetizing the NiMo Ht catalyst was due to the Mo precursor ($

43.5/kg), accounting for 86% of the total catalyst price ($ 38.0/kg) assuming a Mo:Ni ratio of 3:1 as indicated by the XPS analysis, while Ni accounts for only 14% ($ 21.4/kg). Compared to the value of Pt ($ 28,020/kg), the NiMo Ht catalyst can cost approximately 700× less, producing similar current density at the expense of an additional 50 mV overpotential in the current density range investigated here. The NiMo Ht MEC produced stable performance over the duration of the analysis of more that 30 days (Fig. S9). Therefore, the NiMo catalyst developed here represents an inexpensive approach toward stable and high performance MEC. Future studies should focus on the scale up of the technology, producing H_2 from organic matter at the relevant scale.

4. Conclusions

A NiMo catalyst showing superior performance for the HER was synthesized following either an electron assisted approach or a hydrothermal synthesis method. The hydrothermal preparation route enriched the catalyst surface with Mo atoms, enabling higher performance compared to the electron-assisted synthesis. The largest maximum current density reported to date of 48.2 ± 0.2 A/m^2 was obtained in the polarization curve using the NiMo Ht cathode catalyst in the MEC, while the H_2 productivity was 81 ± 3 L_{H2}/L-d with anode Coulombic efficiency of 105 ± 7% and cathode efficiency of 103 ± 6% at a cell voltage of $V_{cell} = -0.86$ V. Using a reference electrode in an improved MEC design, the cathode resistance (5.3 ± 0.5 mΩ m^2) has been shown to dominate the MEC internal resistance (7.6 ± 0.5 mΩ m^2), contributing by 70% to it, while anode (1.4 ± 0.2 mΩ m^2) and ohmic resistance (0.83 mΩ m^2) together contributed for the remainder. NiMo therefore is an optimal choice for an MEC cathode catalyst since it can produce performance similar to that of a Pt catalyst, but at only a fraction of the cost, facilitating the further development of low-cost large-scale cathodes.

CRediT authorship contribution statement

Ruggero Rossi: conceived the idea, performed the experiments, and prepared the original draft. **Joseph Nicolas:** performed the experiments. **Bruce E. Logan:** conceived the idea. All authors revised the manuscript.

Declaration of competing interest

The authors declare that they have no known competing financial interests or personal relationships that could have appeared to influence the work reported in this paper.

Data availability

Data will be made available on request.

Acknowledgements

This work was supported by the U.S. Department of Energy Office of Energy Efficiency and Renewable Energy (EERE) under the award DE-EE0009623. The authors are grateful to J. Shallenberger and J. Anderson for assistance with the XPS and SEM analysis. The authors acknowledge Dr. Frauke Kracke for insight into the electrochemical NiMo synthesis.

Appendix A. Supplementary data

Supplementary data to this article can be found online at https://doi.org/10.1016/j.jpowsour.2022.232594.

References

[1] B.E. Logan, R. Rossi, A. Ragab, P.E. Saikaly, Electroactive microorganisms in bioelectrochemical systems, Nat. Rev. Microbiol. 17 (2019) 307–319, https://doi.org/10.1038/s41579-019-0173-x.
[2] R. Rousseau, L. Etcheverry, E. Roubaud, R. Basséguy, M.L. Délia, A. Bergel, Microbial electrolysis cell (MEC): strengths, weaknesses and research needs from electrochemical engineering standpoint, Appl. Energy 257 (2020), 113938, https://doi.org/10.1016/j.apenergy.2019.113938.
[3] L. Tian, X. Yan, D. Wang, Q. Du, Y. Wan, L. Zhou, T. Li, C. Liao, N. Li, X. Wang, Two key Geobacter species of wastewater-enriched electroactive biofilm respond differently to electric field, Water Res. 213 (2022), https://doi.org/10.1016/j.watres.2022.118185.
[4] B.E. Logan, D. Call, S. Cheng, H.V.M. Hamelers, T.H.J.A. Sleutels, A.W. Jeremiasse, R.A. Rozendal, Microbial electrolysis cells for high yield hydrogen gas production from organic matter, Environ. Sci. Technol. 42 (2008) 8630–8640, https://doi.org/10.1021/es801553z.
[5] L. Lu, Z.J. Ren, Microbial electrolysis cells for waste biorefinery: a state of the art review, Bioresour. Technol. 215 (2016) 254–264, https://doi.org/10.1016/j.biortech.2016.03.034.
[6] C. Santoro, C. Arbizzani, B. Erable, I. Ieropoulos, Microbial fuel cells: from fundamentals to applications. A review, J. Power Sources 356 (2017) 225–244, https://doi.org/10.1016/j.jpowsour.2017.03.109.
[7] X. Wang, S. Cheng, Y. Feng, M.D. Merrill, T. Saito, B.E. Logan, Use of carbon mesh anodes and the effect of different pretreatment methods on power production in microbial fuel cells, Environ. Sci. Technol. 43 (2009) 6870–6874.
[8] J. Tang, Y. Bian, S. Jin, D. Sun, Z.J. Ren, Cathode material development in the past decade for H2 production from microbial electrolysis cells, ACS Environmental Au 2 (2022) 20–29, https://doi.org/10.1021/acsenvironau.1c00021.
[9] X.Y. Zhang, J.Y. Xie, Y. Ma, B. Dong, C.G. Liu, Y.M. Chai, An overview of the active sites in transition metal electrocatalysts and their practical activity for hydrogen evolution reaction, Chem. Eng. J. 430 (2022), https://doi.org/10.1016/j.cej.2021.132312.
[10] Y. Qiu, S. Liu, C. Wei, J. Fan, H. Yao, L. Dai, G. Wang, H. Li, B. Su, X.H. Guo, Synergistic effect between platinum single atoms and oxygen vacancy in MoO2 boosting pH-Universal hydrogen evolution reaction at large current density, Chem. Eng. J. 427 (2022), https://doi.org/10.1016/j.cej.2021.131309.
[11] P.A. Selembo, M.D. Merrill, B.E. Logan, Hydrogen production with nickel powder cathode catalysts in microbial electrolysis cells, Int. J. Hydrogen Energy 35 (2010) 428–437, https://doi.org/10.1016/j.ijhydene.2009.11.014.
[12] L.D.S. Munoz, B. Erable, L. Etcheverry, J. Riess, R. Basséguy, A. Bergel, Combining phosphate species and stainless steel cathode to enhance hydrogen evolution in microbial electrolysis cell (MEC), Electrochem. Commun. 12 (2010) 183–186, https://doi.org/10.1016/j.elecom.2009.11.017.
[13] M. Schalenbach, O. Kasian, K.J.J. Mayrhofer, An alkaline water electrolyzer with nickel electrodes enables efficient high current density operation, Int. J. Hydrogen Energy 43 (2018) 11932–11938, https://doi.org/10.1016/j.ijhydene.2018.04.219.
[14] K.Y. Kim, W. Yang, B.E. Logan, Regenerable nickel-functionalized activated carbon cathodes enhanced by metal adsorption to improve hydrogen production in picrobial electrolysis cells, Environ. Sci. Technol. 52 (2018) 7131–7137, https://doi.org/10.1021/acs.est.7b06005.
[15] K.Y. Kim, S.E. Habas, J.A. Schaidle, B.E. Logan, Application of phase-pure nickel phosphide nanoparticles as cathode catalysts for hydrogen production in microbial electrolysis cells, Bioresour. Technol. 293 (2019), 122067, https://doi.org/10.1016/j.biortech.2019.122067.
[16] J. Zhang, T. Wang, P. Liu, Z. Liao, S. Liu, X. Zhuang, M. Chen, E. Zschech, X. Feng, Efficient hydrogen production on MoNi 4 electrocatalysts with fast water dissociation kinetics, Nat. Commun. 8 (2017), https://doi.org/10.1038/ncomms15437.
[17] M. Schalenbach, F.D. Speck, M. Ledendecker, O. Kasian, D. Goehl, A.M. Mingers, B. Breitbach, H. Springer, S. Cherevko, K.J.J. Mayrhofer, Nickel-molybdenum alloy catalysts for the hydrogen evolution reaction: activity and stability revised, Electrochim. Acta 259 (2018) 1154–1161, https://doi.org/10.1016/j.electacta.2017.11.069.
[18] Y. Zhou, T. Lin, X. Luo, Z. Yan, J. Wu, J. Wang, Y. Shen, Mechanistic study on nickel-molybdenum based electrocatalysts for the hydrogen evolution reaction, J. Catal. 388 (2020) 122–129, https://doi.org/10.1016/j.jcat.2020.05.011.
[19] F. Safizadeh, E. Ghali, G. Houlachi, Electrocatalysis developments for hydrogen evolution reaction in alkaline solutions - a Review, Int. J. Hydrogen Energy 40 (2015) 256–274, https://doi.org/10.1016/j.ijhydene.2014.10.109.
[20] M. Zeng, Y. Li, Recent advances in heterogeneous electrocatalysts for the hydrogen evolution reaction, J Mater Chem A Mater 3 (2015) 14942–14962, https://doi.org/10.1039/c5ta02974k.
[21] B.P. Cario, R. Rossi, K.Y. Kim, B.E. Logan, Applying the electrode potential slope method as a tool to quantitatively evaluate the performance of individual microbial electrolysis cell components, Bioresour. Technol. 287 (2019), 121418, https://doi.org/10.1016/j.biortech.2019.121418.
[22] R. Rossi, D.M. Hall, X. Wang, J.M. Regan, B.E. Logan, Quantifying the factors limiting performance and rates in microbial fuel cells using the electrode potential slope analysis combined with electrical impedance spectroscopy, Electrochim. Acta 348 (2020), 136330, https://doi.org/10.1016/j.electacta.2020.136330.
[23] R. Rossi, B.P. Cario, C. Santoro, W. Yang, P.E. Saikaly, B.E. Logan, Evaluation of electrode and solution area-based resistances enables quantitative comparisons of factors impacting microbial fuel cell performance, Environ. Sci. Technol. 53 (2019) 3977–3986, https://doi.org/10.1021/acs.est.8b06004.

[24] B.E. Logan, E. Zikmund, W. Yang, R. Rossi, K.-Y. Kim, P.E. Saikaly, F. Zhang, Impact of ohmic resistance on measured electrode potentials and maximum power production in microbial fuel cells, Environ. Sci. Technol. 52 (2018) 8977–8985, https://doi.org/10.1021/acs.est.8b02055.
[25] Y. Gu, H. Feng, X. Ying, K. Chen, J. Cheng, H. Huang, S. Zhen, D. Shen, Effects of electrolyte conductivity on power generation in bio-electrochemical systems, Ionics 23 (2017) 2069–2075, https://doi.org/10.1007/s11581-017-2047-4.
[26] S.C. Popat, C.I. Torres, Critical transport rates that limit the performance of microbial electrochemistry technologies, Bioresour. Technol. 215 (2016) 265–273, https://doi.org/10.1016/j.biortech.2016.04.136.
[27] C.I. Torres, A.K. Marcus, B.E. Rittmann, Proton transport inside the biofilm limits electrical current generation by anode-respiring bacteria, Biotechnol. Bioeng. 100 (2008) 872–881, https://doi.org/10.1002/bit.21821.
[28] S.C. Popat, D. Ki, B.E. Rittmann, C.I. Torres, Importance of OH− transport from cathodes in microbial fuel cells, ChemSusChem 5 (2012) 1071–1079, https://doi.org/10.1002/cssc.201100777.
[29] M. Zeppilli, P. Paiano, C. Torres, D. Pant, A critical evaluation of the pH split and associated effects in bioelectrochemical processes, Chem. Eng. J. 422 (2021), https://doi.org/10.1016/j.cej.2021.130155.
[30] R. Rossi, G. Baek, B.E. Logan, Vapor-fed cathode microbial electrolysis cells with closely spaced electrodes enables greatly improved performance, Environ. Sci. Technol. 56 (2022) 1211–1220, https://doi.org/10.1021/acs.est.1c06769.
[31] P. Chen, X. Hu, High-efficiency anion exchange membrane water electrolysis employing non-noble metal catalysts, Adv. Energy Mater. 10 (2020), https://doi.org/10.1002/aenm.202002285.
[32] F. Kracke, J.S. Deutzmann, W. Gu, A.M. Spormann, In situelectrochemical H2 production for efficient and stable power-to-gas electromethanogenesis, Green Chem. 22 (2020) 6194–6203, https://doi.org/10.1039/d0gc01894e.
[33] F. Kracke, A.B. Wong, K. Maegaard, J.S. Deutzmann, M.K.A. Hubert, C. Hahn, T. F. Jaramillo, A.M. Spormann, Robust and biocompatible catalysts for efficient hydrogen-driven microbial electrosynthesis, Commun Chem 2 (2019), https://doi.org/10.1038/s42004-019-0145-0.
[34] Y. Wang, Y. Wang, J. Bai, W.M. Lau, Efficient self-supported bifunctional NiMo alloy electrocatalysts for water splitting in alkaline environment, ChemistrySelect 7 (2022), https://doi.org/10.1002/slct.202200468.
[35] T. Wang, R. Jin, X. Wu, J. Zheng, X. Li, K. Ostrikov, A highly efficient Ni-Mo bimetallic hydrogen evolution catalyst derived from a molybdate incorporated Ni-MOF, J Mater Chem A Mater 6 (2018) 9228–9235, https://doi.org/10.1039/c8ta01325j.
[36] M. Mitov, E. Chorbadzhiyska, L. Nalbandian, Y. Hubenova, Nickel-based electrodeposits as potential cathode catalysts for hydrogen production by microbial electrolysis, J. Power Sources 356 (2017) 467–472, https://doi.org/10.1016/j.jpowsour.2017.02.066.
[37] M.P. Seah, Summary of ISO/TC 201 standard: VII ISO 15472 : 2001 - surface chemical analysis - x-ray photoelectron spectrometers - calibration of energy scales, Surf. Interface Anal. 31 (2001) 721–723, https://doi.org/10.1002/sia.1076.
[38] J.R. Ambler, B.E. Logan, Evaluation of stainless steel cathodes and a bicarbonate buffer for hydrogen production in microbial electrolysis cells using a new method for measuring gas production, Int. J. Hydrogen Energy 36 (2011) 160–166, https://doi.org/10.1016/j.ijhydene.2010.09.044.
[39] B.E. Logan, B. Hamelers, R. Rozendal, U. Schröder, J. Keller, S. Freguia, P. Aelterman, W. Verstraete, K. Rabaey, Microbial fuel cells: Methodology and technology, Environ. Sci. Technol. 40 (2006) 5181–5192, https://doi.org/10.1021/es0605016.
[40] J.A. Bau, S.M. Kozlov, L.M. Azofra, S. Ould-Chikh, A.H. Emwas, H. Idriss, L. Cavallo, K. Takanabe, Role of oxidized Mo species on the active surface of Ni-Mo electrocatalysts for hydrogen evolution under alkaline conditions, ACS Catal. 10 (2020) 12858–12866, https://doi.org/10.1021/acscatal.0c02743.
[41] R. Bernasconi, M.I. Khalil, D.S. Cakmakci, Y. Bektas, L. Nobili, L. Magagnin, C. Lenardi, Electrocatalytic layers for hydrogen evolution reaction based on nickel phosphides: cost-effective fabrication and XPS characterization, J. Mater. Sci. 57 (2022) 9370–9388, https://doi.org/10.1007/s10853-022-07251-3.
[42] X. Zhang, W. He, L. Ren, J. Stager, P.J. Evans, B.E. Logan, COD removal characteristics in air-cathode microbial fuel cells, Bioresour. Technol. 176 (2015) 23–31, https://doi.org/10.1016/j.biortech.2014.11.001.